Comparison of Local and Global Stability of an Analogue of a Disulfide-Folding Intermediate with Those of the Wild-Type Protein in Bovine Pancreatic Ribonuclease A: Identification of Specific Regions of Stable Structure along the Oxidative Folding Pathway†

John H. Laity,‡,§ Gaetano T. Montelione,*,‖ and Harold A. Scheraga*,‡

Baker Laboratory of Chemistry and Chemical Biology, Cornell University, Ithaca, New York 14853-1301, and Center for Advanced Biotechnology and Medicine and Department of Molecular Biology and Biochemistry, Rutgers University, Piscataway, New Jersey 08854-5638

Received May 20, 1999; Revised Manuscript Received October 14, 1999

ABSTRACT: We have identified specific regions of the polypeptide chain of bovine pancreatic ribonuclease A (RNase A) that are critical for stabilizing the oxidative folding intermediate des-[40−95] (with three native disulfide bonds but lacking the fourth native Cys40−Cys95 disulfide bond) in an ensemble of largely disordered three-disulfide precursors (3S ⇔ des-[40−95]). A stable analogue of des-[40−95], viz., [C40A, C95A] RNase A, which contains three out of four native disulfide pairings, was previously found to have a three-dimensional structure very similar to that of the wild-type protein. However, it is determined here from GdnHCl denaturation experiments to have significantly reduced *global* stability, i.e., $[\Delta\Delta G^{\circ}_{unf}(H_2O)]_{wild\text{-}type-[C40A,C95A]} = 4.5$ kcal /mol at 20 °C and pH 4.6. The *local* stability of [C40A, C95A] RNase A was also examined using site-specific amide $^2H/^1H$ exchange measurements at pD 5.0 to determine the individual unfolding free energy of specific residues (ΔG°_{op}), under both strongly native (12 °C) and more destabilizing (20 °C) conditions. Comparison of the relative stabilities [$\Delta G^{\circ}_{op}/\Delta G^{\circ}_{unf}(H_2O)$] at specific amide sites of [C40A, C95A] RNase A at both temperatures with the corresponding values for the wild-type protein at 35 °C corroborates previous experimental evidence that unidentified intramolecular contacts in the vicinity of the preferentially formed native one-disulfide (C65−C72) loop are crucial for stabilizing early folding intermediates, leading to des-[40−95]. Moreover, values of ΔG°_{op} for residues at or near the third α-helix, and in part of the second *β*-sheet of [C40A, C95A] RNase A, indicate that these two regions of regular backbone structure contribute to stabilizing the global chain fold of the des-[40−95] disulfide-folding intermediate in the wild-type protein. More significantly, we have identified numerous specific residues in the first α-helix and the first *β*-sheet of the protein that are stabilized in the final step of the major oxidative regeneration pathway of RNase A (des-[40−95] ⇒ N).

Considerable information has been obtained from thermodynamic and kinetic studies of the oxidative folding of bovine pancreatic ribonuclease A (RNaseA[1]) (*1*−*7*). In the presence of dithiothreitol (DTT), this 124-residue protein (with disulfide bonds at positions 26−84, 40−95, 58−110, and 65−72) folds through pathways (shown in Figure 1) involving a rapid preequilibrium resulting in an ensemble of 3S species, followed by two dominant major and minor rate-determining steps in which the specific three-disulfide species, des-[40−95] and des-[65−72], respectively, are formed by disulfide reshuffling (*7*). These des-RNase A species, with three native disulfide bonds, are also formed in two other "very minor" redox-dependent pathways (*8*, *9*). Most of the conformational folding occurs in the rate-determining steps that generate des-[40−95] and des-[65−72].

To determine the molecular events that govern the stages of the oxidative folding mechanism in RNase A, we have used heteronuclear NMR methods to characterize and compare the three-dimensional structures of wild-type RNase A and stable analogues of the three-disulfide des species in which the Cys65/Cys72 (*10*) and Cys40/Cys95 (*11*) residues have been replaced by serine and alanine residues, respec-

† This work was supported by grants from the National Institutes of Health (GM-24893 to H. A. S., and GM-50733 to G. T. M.) and the National Foundation for Cancer Research (to H. A. S.). J. H. L. was an NIH predoctoral trainee at Cornell.

‡ Cornell University.

§ Present address: Department of Molecular Biology (MB-2), The Scripps Research Institute, La Jolla, California 92037.

‖ Rutger University.

* Address correspondence to H. A. Scheraga. Telephone: 607-255-4034. Fax: 607-254-4700. E-mail: has5@cornell.edu.

[1] Abbreviations: RNase A, bovine pancreatic ribonuclease A; [C40A, C95A] RNase A, three-disulfide mutant of RNase A, in which cysteines 40 and 95 are replaced by alanines; des-[40−95] and des-[65−72], three-disulfide species of RNase A with native disulfide bonds C26−C84 and C58−C110, but lacking either the C40−C95 (des-[40−95]) or the C65−C72 (des-[65−72]) disulfide bond; PDLA, poly-DL-alanine; DTT^{ox}, oxidized DL-dithiothreitol; DTT^{red}, reduced DL-dithiothreitol; GdnHCl, guanidinium hydrochloride; OD_{610}, optical density at 610 nm; OD_{287}, optical density at 287 nm; 2D, 2-dimensional; $^2H/^1H$ exchange, amide deuterium/hydrogen exchange; HSQC, heteronuclear single quantum coherence; NOE's, cross-peaks observed in nuclear Overhauser effect spectroscopy; PFG, pulsed-field gradient; pD_{read}, pH meter reading of a ^2H_2O solution, $pD = -\log[^2H_3O^+]$.

10.1021/bi9911684 CCC: $18.00
Published on Web 11/24/1999

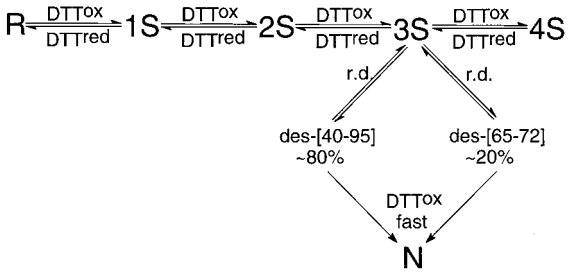

FIGURE 1: Schematic representation of the regeneration pathways of RNase A in the presence of a redox couple (DTT^{ox}/DTT^{red}) at 20 °C and pH 8.0 (*7*). R, N, 1S, 2S, 3S, and 4S represent the reduced (R), native (N), and all the respective folding intermediates containing differing numbers, 1−4, of disulfide bonds, S. Although some of the 1S, 2S, 3S, and 4S folding intermediates have some local secondary structure, they lack the global chain fold of native wild-type RNase A. des-[40−95] and des-[65−72] are the dominant structural intermediates formed in the major (∼80%) and minor (∼20%) rate-determining (r.d.) regeneration pathways, respectively. Both des-[40−95] and des-[65−72] are folded protein forms with nativelike, but less stable structures, than native wild-type RNase A (see refs *10* and *11* for a detailed stuctural comparison of analogues of des-[40−95] and des-[65−72], respectively, with the native wild-type protein).

tively. Comparisons of chemical shift, nuclear Overhauser effect, scalar coupling, and other NMR data obtained for these des species with NMR data obtained for wild-type RNase A identifies the structural differences between these three-disulfide and wild-type species (*10, 11*). This information, however, is not sufficient to characterize all of the energetic contributions to the final folding steps in which the fourth missing disulfide bond is formed. For this purpose, it is also necessary to obtain information about changes in global and local conformational fluctuations of these des and wild-type species. Such dynamic information complements the information already available from kinetic studies (*7*−*9*) about the relative rates and tendencies of the des species to oxidize to the native structure or reshuffle back to the three-disulfide ensemble 3S (Figure 1), and from the structural data derived from NMR studies (*10, 11*).

Protein conformational dynamics can be characterized by several different NMR methods, each of which probes internal motions on different time scales. This paper describes efforts to characterize changes in conformational dynamics and local structural stability associated with the final step in the major oxidative folding pathway, involving conversion of the three-disulfide species des [40−95] into the four-disulfide native RNase A (N), using amide hydrogen−deuterium exchange measurements. Specifically, guanidine hydrochloride (GdnHCl) denaturation and amide hydrogen−deuterium exchange measurements are compared in order to characterize the global unfolding free energies [ΔG°_{unf} (H_2O)] and the local, individual-residue, unfolding free energies (ΔG°_{op}), respectively, of des [40−95] and wild-type RNase A. The relative contributions of these free energies in the final stage of the major oxidative folding pathway of RNase A in which des [40−95] is converted to N (Figure 1), are discussed.

MATERIALS AND METHODS

Materials. Ultrapure GdnHCl was obtained from ICN Biochemicals and purified further by recrystallization as described elsewhere (*12*). Deuterated solvents were from Cambridge Isotope Labs, and all other reagents were of the highest quality commercially available.

Expression and Purification of [C40A, C95A] and Wild-Type RNase A Proteins. Construction of the DNA vectors pRM[C40A, C95A] (*11, 13*) and pXBR-2 (*14*), used to express recombinant [C40A, C95A] RNase A and wild-type RNase A, has been described previously. Uniformly isotopically ^{15}N-enriched [C40A, C95A] RNase A and wild-type RNase A were expressed, purified, and characterized as described by Laity et al. (*11*). The method for expression of un-enriched [C40A, C95A] RNase A and wild-type RNase A used in GdnHCl unfolding experiments was identical to that for expression of enriched protein, except that the inoculate was diluted directly into 1 L of LB media containing 50 μg/mL ampicillin and 0.01% (w/v) thiamine hydrochloride. The cell induction at OD_{610}, amount of IPTG added, cell growth time after induction, and external growth conditions were the same as those used in the expression of the enriched protein (*11, 13*).

pH and pD Measurements. All pH and pD measurements were made using a Radiometer America pH meter with a Beckman KCl electrode. The specific deuterium isotope effect was determined for this electrode using HCl and DCl solutions, and is described by

$$pD = pD_{read} + 0.4 \quad (1)$$

where pD_{read} was the observed, uncorrected "pH" reading displayed on the instrument. This deuterium isotope correction is consistent with that reported previously by Glasoe and Long (*15*).

Guanidinium Hydrochloride Transitions. Three solutions were used to prepare the samples: (i) a buffer solution of 100 mM sodium acetate pH 4.60 ± 0.03, (ii) a protein solution of ∼70 μM (∼1 mg/mL) wild-type or [C40A, C95A] RNase A in 100 mM sodium acetate pH 4.60 ± 0.03, and (iii) an 8 M GdnHCl solution in 100 mM sodium acetate pH 4.60 ± 0.03. Accurate concentrations of GdnHCl were determined using a Bausch and Lomb refractometer (*12*). Reversible protein unfolding was observed by monitoring $\Delta\epsilon_{287}$ by absorbance, using a modified Cary 14 spectrophotometer (*16*), and all spectroscopic measurements were made in quartz cuvettes. An equal number of samples was prepared under denaturing (solutions 1 and 2 mixed first, with solution 3 added later) and renaturing (solutions and 2 and 3 mixed first, with solution 1 added later) conditions, and left to equilibrate for 12 h. This procedure was necessary to determine the reversibility of the protein denaturation using GdnHCl. The sample temperature was controlled by a Neslab (Portsmouth, NH) RTE−100 thermal water bath, which provided constant circulation through a block holding the cuvette. Sample temperatures of 12, 16, 20, and 24 °C for [C40A, C95A] RNase A, and 20, 25, 30, and 35 °C for wild-type RNase A were calibrated before data measurements were made by placing a National Bureau of Standards thermometer directly in a cuvette filled with H_2O (placed inside the water-circulated block), whereby the correct setting for the thermal water bath temperature regulator was determined. Solutions were equilibrated for 10 min at each target temperature prior to OD_{287} measurement. Thermodynamic parameters were determined from the GdnHCl denaturation data using the nonlinear curve fitting method of

Santoro and Bolen (*17*). All unfolding curves were analyzed with Kaleidagraph (Synergy Software).

NMR Sample Preparation. Solutions of uniformly ^{15}N-enriched [C40A, C95A] and wild-type RNase A samples were prepared by dissolving lyophilized protein in 90/10% ($^1H_2O/^2H_2O$) for measurements of the temperature or pH dependence of the chemical shifts, or 99.99% ^2H_2O for $^2H/^1H$ exchange measurements. All NMR experiments were carried out in 5 mm susceptibility-matched Shigemi NMR tubes sealed with Parafilm. The ^{15}N-enriched [C40A, C95A] RNase A and wild-type RNase A sample concentrations ranged from 3.5 to 4.5 mM. An extensive set of backbone and some side-chain-resonance assignments have been reported previously for both wild-type (*10*) and [C40A, C95A] (*11*) RNase A.

Amide $^2H/^1H$ Exchange Rates. All 2D ^{15}N−HSQC experiments were carried out on a Varian Unity 500 NMR spectrometer at Cornell, equipped with three full channels and computer controlled temperature regulation. Phase-sensitive data were acquired by combining n- and p- spectra (*18*, *19*) selected with pulse-field gradients (PFG's). The ^{1}H and ^{15}N chemical shifts were referenced with respect to 2,2-dimethyl-2-silapentane-5-sulfonic acid (DSS) as an internal standard using the protocol recommended by the IUPAC-IUBMB-IUPAB Interunion Task Group on NMR Data Bases (*20*).

Backbone amide proton exchange rate constants for uniformly ^{15}N-enriched [C40A, C95A] RNase A and wild-type RNase A were measured by heteronuclear NMR using the methods described previously (*10, 11, 21*). Briefly, continuous sequential acquisition at sucessive time intervals of at least 90 ^{15}N-^{1}H PFG-HSQC spectra were used to monitor amide $^2H/^1H$ exchange. All spectra were acquired with 192 × 2048 complex data points in the t_1 and t_2 dimensions, respectively, and 4 scans per t_1 increment, using a total experiment time of thirty-nine minutes per 2D spectrum. The ^{15}N-^{1}H PFG-HSQC spectra were processed on a Sun LX workstation. A Gaussian window function and baseline correction were applied in both dimensions, and zero filling was used to extend the time-domain data further in the t_1 dimension to a final 2D matrix size of 512 × 2048 in the t_1 and t_2 dimensions, respectively. Identical processing and peak picking parameters using FELIX software, coupled with semi-automated custom FELIX computer programs, were used to determine individual proton peak intensities [$I(t)$] as a function of time t. The extrinsic amide exchange rate constant, k_{ex}, was then determined by using a least-squares fit to

$$\ln I(t) = \ln[I_0] - k_{ex}(t) \qquad (2)$$

which describes the natural logarithm of the peak intensity as a linear function of time. Poor quality data near the base of the exponential decay curve were truncated for those residues with relatively large $^2H/^1H$ rate constants (k_{ex} is approximately equal to or greater than 5×10^{-5} sec^{-1}). Generally, conversion of data to their natural logarithm and plotting the data as a function of time facilitated the determination of where to truncate the noisy data.

Determination of ΔG°_{op} From Measured Extrinsic Amide Exchange Rate Constants. The following expressions define the amide proton exchange rate constants (*22*) for a protein with ^{1}H protons that has been dissolved in ^2H_2O:

$$k_{ex} = k_{op}\, k_{int}[D]/(k_{op} + k_{cl} + k_{int}[D]) \text{ with } (D = D^+, OD^-, D_2O) \qquad (3)$$

$$k_{int}[D] = k_{acid}[D^+] + k_{base}[OD^-] + k_{D_2O}[D_2O]$$

where [D] is the concentration of ^2H_2O in its various catalytic forms, k_{op} and k_{cl} are the "opening" and "closing" rate constants, respectively, for an amide proton otherwise protected from solvent, and k_{int} is the "intrinsic" rate constant for solvent-exposed $^2H/^1H$ exchange. Limiting exchange mechanisms (EX1 and EX2) are described in eqs 4, a and b, respectively.

$$k_{ex} \cong k_{op} \quad (\text{EX1; } k_{int}[D] \gg k_{cl} \text{ and } k_{int}[D] \gg k_{op}) \qquad (4a)$$

$$k_{ex} \cong K_{op}\, k_{int}[D] \quad (\text{EX2; } k_{cl} \gg k_{int}[D] \text{ and } K_{op} \ll 1) \qquad (4b)$$

where $K_{op} = k_{op} / k_{cl}$ is the equilibrium constant that characterizes the solvent accessibility (and the local conformational stability monitored by an individual amide proton site). For slowly exchanging amide sites, the EX2 mechanism (*22*) described in eq 4b is almost always observed (*23*−*25*). For completeness, the EX1 limit (eq 4a) (*22*) will also be considered in our analysis of these amide proton exchange data. Eq 5 describes the corresponding unfolding free energy (ΔG°_{op}) (*24*) that can be derived from k_{ex} and $k_{int}[D]$ in the EX2 limit (eq 4b).

$$\Delta G^\circ_{op} = -RT \ln K_{op} = -RT \ln(k_{ex}/k_{int}[D]) \qquad (5)$$

To calculate solvent accessible intrinsic amide exchange rates ($k_{int}[D]$) for individual protonated residues of a protein in D_2O, the measured rates for poly-DL-alanine (PDLA) at 20 °C as a function of pD (*26*) were used. Corrections for inductive and steric effects of neighboring side chains, first measured by Molday et al. (*26*), and later improved using model peptides by Bai et al. (*27*), were then applied to the PDLA rate to determine the resulting intrinsic rate, $k_{int}[D]$. Finally, to determine intrinsic amide exchange rates for individual protonated residues of a protein in D_2O at a temperature (T) other than 20 °C (293 K), experimentally determined activation energies (E_a) (*28*−*30*) were used in eq 6. Values for E_a of 14, 17, and 19 kcal/mol were used for the k_{acid}, k_{base}, and k_{D_2O} rate constants, respectively (27).

$$k_{ex}(T) = k_{ex}(293) \exp[-E_a(1/T - 1/293)] \qquad (6)$$

RESULTS

GdnHCl Transitions. GdnHCl denaturation curves that were determined for both wild-type (20, 25, 30, and 35 °C) and [C40A, C95A] RNase A (12, 16, 20, and 24 °C) at pH 4.60 are shown in Figure 2. The corresponding thermodynamic data computed from these curves are presented in Table 1. The difference in the values of $\Delta G^\circ_{unf}(H_2O)$ between wild-type RNase A and [C40A, C95A] RNase A [$\Delta\Delta G^\circ_{unf}(H_2O)_{\text{wild-type}-[C40A,C95A]} = 4.5$ kcal/mol at 20 °C] is a direct measure of the significant difference in *global* stability between the two proteins. Another indication of conformational differences between the mutant and wild-type proteins comes from the comparison of the slopes of

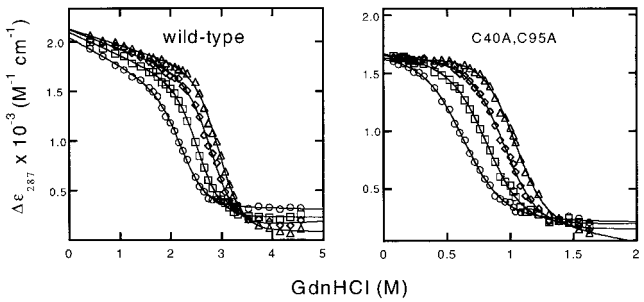

FIGURE 2: GdnHCl unfolding curves at pH 4.60 with $\Delta\epsilon_{287}$ [$\epsilon_{287(H_2O)} - \epsilon_{287\ (GdnHCl\ denatured)}$] for wild-type (left) and [C40A, C95A] RNase A (right) plotted as function of temperature. Curves were measured at 20 °C (△), 25 °C (◇), 30 °C (□), and 35 °C (○) for wild-type, and at 12 °C (△), 16 °C (◇), 20 °C (□), and 24 °C (○) for [C40A, C95A] RNase A. The solid lines represent nonlinear fits to the raw data using the method of Santoro & Bolen (17).

Table 1. Parameters Characterizing the GdnHCl Unfolding of [C40A, C95A] RNase A and Wild-Type RNase A at pH 4.60

protein form (RNase A)	temperature (°C)	m (kcal mol^{-1} M^{-1})	$\Delta G°_{unf}(H_2O)$ (kcal mol^{-1})	$[GdnHCl]^{1/2}$ (M)
wild-type	20	2.68 ± 0.29[a]	7.93[b] ± 0.80	2.96 ± 0.15
wild-type	25	2.56 ± 0.29	7.22 ± 0.81	2.82 ± 0.16
wild-type	30	2.65 ± 0.20	6.59 ± 0.50	2.56 ± 0.11
wild-type	35	2.48 ± 0.26	5.60 ± 0.61	2.25 ± 0.15
[C40A,C95A]	12	4.66 ± 0.59	4.79 ± 0.54	1.00 ± 0.17
[C40A,C95A]	16	4.47 ± 0.56	4.26 ± 0.50	0.95 ± 0.17
[C40A,C95A]	20	4.08 ± 0.65	3.38 ± 0.55	0.83 ± 0.23
[C40A,C95A]	24	3.83 ± 0.58	2.40 ± 0.50	0.63 ± 0.26

[a] All uncertainties are reported at the 95% confidence limit. [b] Not including the 1.7 kcal/mol correction for proline isomerization (see Results for an explanation of this correction).

their respective unfolding curves, m_{GdnHCl} (Table 1), which are a measure of the change in exposed surface area of a protein upon GdnHCl-induced unfolding (*31*). This value is significantly larger for [C40A, C95A] RNase A than for the wild-type protein ($\Delta m_{GdnHCl(wild\text{-}type-[C40A,C95A])}$) = −1.4 kcal mol^{-1} M^{-1} at 20 °C), which suggests that the des analogue has greater solvent accessiblity in the *unfolded* state than unfolded wild-type RNase A; the alternative interpretation, that the des analogue is more compact than wild-type RNase A in their respective *folded* states, is ruled out by the experimental NMR data available for both of these species (*10*, 11). These GdnHCl stability data for wild-type and [C40A, C95A] RNase A provide a basis for direct comparisons of the global unfolding free energy $\Delta G_{unf}(H_2O)$ with individual values of $\Delta G°_{op}$ for each amide resonance observed in the 2D $^{15}N-HSQC$ spectrum of the respective proteins.

Non-native Proline Isomers in Denatured RNase A. The free energy of unfolding includes the free energy of cis/trans isomerization of X-Pro peptide groups between the native and denatured forms (*32*, *33*). While this free-energy change is included in thermodynamic measurements of protein unfolding, the unfolded state probed by amide $^2H/^1H$ exchange studies is a transient species that is generally too short-lived to allow for proline isomerization. For these reasons, comparisons of protein unfolding energetics must be corrected to account for the effect of such isomerizations that contribute to the unfolding free energies measured in equilibrium unfolding studies, but not to those measured by amide $^2H/^1H$-exchange by the EX2 mechanism. This can be done by determining the relative populations of the denatured state molecules in GdnHCl-unfolded RNase A, which exist in the native X-proline isomeric state (*34*−*36*). A correction can be made for non-native proline isomers in denatured wild-type and mutant RNase A by assuming that the concentration of native X-proline peptide groups is the same for both protein forms. In [C40A, C95A] RNase A, Pro42 and Pro93 are near the Ala40 and Ala95 mutation sites, respectively. However, NMR measurements indicate that the X-Pro93 peptide group is cis in both [C40A, C95A] RNase A (*11*) and wild-type RNase A. Furthermore, given that the Asn113−Pro114 peptide group is far from the mutation site in the des-[40−95] analogue, and that the overall structure of the mutant is similar to that of the wild-type protein (*11*), this peptide group also appears to be in the wild-type cis conformation in the folded structure of [C40A, C95A] RNase A. The more energetically favored trans conformation for the Lys41−Pro42 and Val116−Pro117 peptide groups of the wild-type protein are not likely to be altered in the des-[40−95] analogue (*11*). Using the estimated fractions of native X-proline isomers in unfolded wild-type RNase A (*36*), 1.7 kcal/mol must be added to the values of $\Delta G°_{unf}(H_2O)$ determined by GdnHCl unfolding measurements in order to compare them with $\Delta G°_{unf}$values determined by amide $^2H/^1H$ exchange measurements.

Temperature and pH Dependence of ^1H and ^{15}N Chemical Shifts. For the purpose of comparing exchange rate constants (k_{ex}) of the two proteins under comparable stabilizing conditions relative to the transition temperature ($T_m - T \sim$ 20 °C), it was necessary to assign the backbone amide ^1H and ^{15}N chemical shifts for [C40A, C95A] RNase A and wild-type RNase A under these specific solution conditions. Sets of 2D $^{15}N-HSQC$ spectra were acquired at 12, 16, 20, and 24 °C for [C40A, C95A] RNase A, and at 20, 25, 30, and 35 °C for wild-type RNase A. The corresponding ^1H- and ^{15}N-resonance assignments reported previously at 20 °C for wild-type (10) and [C40A, C95A] RNase A (11) were then used, along with their approximately linear dependence of chemical shift on temperature, to determine nearly complete ^1H and ^{15}N resonance assignments for [C40A, C95A] RNase A at 12 °C, and for wild-type RNase A at 35 °C. The slopes ($\Delta\delta/\Delta T$) of the linear least-squares fits to each data set (^1H and ^{15}N) of chemical shifts (in ppm) as a function of temperature are tabulated in Tables S1 and S2 (see Supporting Information) for the wild-type and mutant RNase A, respectively.

Validation of EX2 Mechanism for Amide $^2H/^1H$ Exchange. To confirm the applicability of an EX2 mechanism for $^2H/^1H$ exchange in RNase A at pD 5.0, a set of 2D $^{15}N-HSQC$ spectra were recorded at pH 4.6, 5.0, 5.5, 6.0, 6.5, and 7.0 for the wild-type protein at 35 °C. In contrast to the data for the temperature dependence of the ^1H- and ^{15}N-chemical shifts, the trend of chemical shift change as a function of pH was not always linear for wild-type RNase A, especially for His, Asp, and Glu residues that are often characterized by large changes in chemical shift around their pK_a's. In addition, the resonances of some residues were not visible in spectra recorded at pH 6.5−7.0, most likely because of intermediate exchange effects. However, 35 $^1H-^{15}N$ resonance assignments corresponding to residues that had observable $^2H/^1H$ exchange rates (e.g., visible $^1H-^{15}N$ correlations in the corresponding 2D $^{15}N-HSQC$ spectra recorded in ^2H_2O) were obtained for wild-type RNase A at 35 °C and pH 7.0.

The pD dependence of amide exchange rate constants (k_{ex}'s) were compared for these 35 NH sites of wild-type RNase A at pD 5.0 and pD 7.0 (data not shown). In the base-catalyzed regime of pD 5−7, the EX2 mechanism (*22*) is characterized by a pseudo first-order rate constant (eq 4b) that depends on the opening equilibrium constant (K_{op}), the residue-specific "intrinsic" rate constant k_{int}, and the solvent [OD^-] concentration. By contrast, in an EX1 mechanism (*22*), k_{ex} would be characterized *only* by the opening rate constant ($k_{ex} = k_{op}$) of the corresponding amide residue, which to a first approximation is independent of pH. In fact, the $^2H/^1H$ exchange rate constants measured as a function of pD for wild-type RNase A are characterized by a significant increase from pD 5.0 to pD 7.0 (log $[k_{ex[pD7]}/k_{ex[pD5]}]_{ave} = 1.1$). If the conformational stability of RNase A were independent of pH, an increase from pH 5.0 to 7.0 would correspond to a 100 fold increase in solvent [OD^-] concentration, and a value for log ($k_{ex[pD\ 7]}/k_{ex[pD\ 5]}$) of 2 would be expected. However, it is well-documented that the stability of RNase A increases between pH 4 and 7 (*13, 37*) (and between pD 4 and 5, J. H.L and H. A.S, unpublished results), thus counteracting to various degrees (depending on the change in local stability at each individual NH site), the effect of an increase in solvent [OD^-] concentration over the same pD range. Furthermore, since RNase A is more stable at pD 7.0 than at pD 5.0, k_{ex} would be expected to *decrease* with increasing pD in an EX1 mechanism. Therefore, given the signficant *increase* in k_{ex} with increasing pD for most individual amide sites of RNase A, the analyses in this paper involving the determination of ΔG°_{op}, which are based on an EX2 mechanism, appear to be generally valid.

Determination of ΔG°_{op}. An extensive list of amide $^2H/^1H$ exchange rate constants, measured at pD 5.0 for mutant (at 20 °C and 12 °C) and wild-type RNase A (at 35 °C), is presented in Table 2. Thermal transition measurements reported previously (*10, 11*) confirm that both [C40A, C95A] RNase A and wild-type RNase A are in their respective native conformations at 12 to 20 and 35 °C, respectively, at pH 5. The excellent quality of the measured extrinsic rate constants (k_{ex}), indicated by the low uncertainties in the calculated values (generally <10% at the 95% confidence level), was obtained by choosing relative temperatures ($T_m - T$) for [C40A, C95A] RNase A and wild-type RNase A to measure $^2H/^1H$ exchange rate constants in which k_{ex} values are in the range from 10^{-4} to 10^{-7} sec^{-1}. Each $^2H/^1H$ exchange NMR data set was recorded in 3−5 days. A total of 64 cross-peaks corresponding to slowly exchanging amide protons was observed in the 2D $^{15}N-HSQC$ spectra for wild-type RNase A at 35 °C, while 57 and 62 cross-peaks were observed in the same type of spectra recorded for [C40A, C95A] RNase A at 20 and 12 °C, respectively.

Wild-type RNase A at 35 °C and pD 5.0 exhibits more amide sites with $^2H/^1H$ exchange rates slow enough to be studied than [C40A, C95A] RNase A at 12 or 20 °C and pD 5.0, since wild-type RNase A is more stable [e.g., has a larger $\Delta G^\circ_{unf}(H_2O)$] at 35 °C and pH 4.60, than is [C40A, C95A] RNase A at both 12 and 20 °C and pH 4.60 (see Table 1). Similarly, five residues (Q28, Y97, A109, Y115, and H119) in [C40A, C95A] RNase A at pD 5.0 had $^2H/^1H$ exchange rates slow enough to be observed at 12 but not at 20 °C because of the greater stability of [C40A, C95A] RNase A at 12 compared to 20 °C [$\Delta\Delta G^\circ_{unf}(H_2O)_{[C40A,C95A]12-20\ °C} = 1.41$ kcal/mol, Table 1]. By contrast, the $^2H/^1H$ exchange rate for the Y115 amide

Table 2. Amide $^2H/^1H$ Exchange Rate Constants (k_{ex}) Measured at pD 5.0 for Wild-Type RNase A at 35 °C, and [C40A, C95A] RNase A at 12 °C and 20 °C[a]

residue	wild-type RNase A (35 °C) $k_{ex} \times 10^5$ (sec^{-1})	[C40A, C95A] RNase A (12 °C) $k_{ex} \times 10^5$ (sec^{-1})	[C40A, C95A] RNase A (20 °C) $k_{ex} \times 10^5$ (sec^{-1})
A6	55 ± 46[b]	1.4 ± 0.039	24 ± 8.0
K7	48 ± 14	0.47 ± 0.018	17 ± 2.1
F8	25 ± 7.4	0.20 ± 0.018	13 ± 7.4
E9	3.7 ± 0.18	0.069 ± 0.013	6.4 ± 0.18
R10	1.5 ± 0.22	0.11 ± 0.011	5.2 ± 1.9
Q11	0.26 ± 0.16	0.088 ± 0.019	8.1 ± 1.0
H12	0.75 ± 0.046	0.53 ± 0.062	nd[c]
M13	0.47 ± 0.011	0.43 ± 0.039	11 ± 2.4
D14	0.99 ± 0.050	0.41 ± 0.029	11 ± 5.0
C26	33 ± 23	2.4 ± 0.73	60 ± 45
Q28	2.2 ± 0.14	2.3 ± 0.17	nd[c]
M29	0.61 ±0.037	0.050 ± 0.0040	4.7 ± 4.2
M30	0.15 ± 0.013	0.032 ± 0.028	3.4 ± 1.3
K31	4.1 ± 0.22	0.23 ± 0.013	10 ± 0.86
R33	24 ± 2.7	nd[c]	nd[c]
N34	20 ± 1.4	1.7 ± 0.26	44 ± 12
N44	0.99± 0.052	0.43 ± 0.019	2.5 ± 2.2
F46	0.25 ± 0.021	0.072 ± 0.0052	6.8 ± 1.7
V47	0.13 ± 0.017	0.076 ± 0.0036	2.6 ± 0.69
H48	0.32 ± 0.029	0.22 ± 0.034	8.7 ± 3.2
E49	2.1 ± 0.17	0.27 ± 0.017	18 ± 2.0
L51	0.14 ± 0.015	0.47 ± 0.018	15 ± 12
D53	34 ± 6.4	3.7 ± 0.30	10 ± 2.1
V54	0.30 ± 0.020	0.011 ± 0.0034	0.82 ± 0.088
Q55	0.19 ± 0.013	0.032 ± 0.0029	1.7 ± 0.37
A56	0.51 ± 0.021	0.038 ± 0.0015	3.0 ± 0.65
V57	0.17 ± 0.019	0.0062 ± 0.0015	0.99 ± 0.12
C58	0.24 ± 0.024	0.052 ± 0.0040	4.2 ± 0.36
S59	0.99 ± 0.033	0.11 ± 0.0033	4.8 ± 0.55
Q60	0.33 ± 0.024	0.12 ± 0.0040	5.4 ± 0.83
K61	0.73 ± 0.025	0.10 ± 0.0040	3.1 ± 1.1
V63	0.14 ± 0.018	0.020 ± 0.0015	2.0 ± 0.26
A64	nd[c]	8.9 ± 2.0	22 ± 14
C65	13 ± 1.0	0.43 ± 0.018	8.1 ± 2.2
C72	0.22 ± 0.014	0.078 ± 0.0028	3.6 ± 0.57
Y73	0.10 ± 0.020	1.1 ± 0.10	6.3 ± 1.5
Q74	0.12 ± 0.021	0.056 ± 0.0032	3.8 ± 1.4
S75	0.13 ± 0.019	0.047 ± 0.0078	4.4 ± 2.0
Y76	11 ± 2.7	0.31 ± 0.018	8.6 ± 1.8
M79	0.076 ± 0.021	0.066 ± 0.0035	5.7 ± 1.5
I81	0.073 ± 0.026	0.058 ± 0.0039	3.6 ± 0.026
T82	0.057 ± 0.020	0.053 ± 0.0034	3.7 ± 0.80
D83	8.6 ± 0.61	0.70 ± 0.051	8.2 ± 3.2
C84	1.0 ± 0.029	nd[c]	nd[c]
R85	2.8 ± 0.84	0.73 ± 0.13	12 ± 3.5
A96	17 ± 8.8	nd[c]	nd[c]
Y97	3.4 ± 0.40	2.91 ± 0.76	nd[c]
K98	0.10 ± 0.014	1.11 ± 0.13	20 ± 11
T100	0.18 ± 0.020	0.54 ± 0.15	11 ± 1.9
A102	0.28 ± 0.074	0.45 ± 0.033	20 ± 5.7
K104	0.30 ± 0.020	0.0090 ± 0.011	7.0 ± 1.7
I106	0.044 ± 0.0081	0.0086 ± 0.0040	4.7 ± 0.68
I107	0.13 ± 0.015	0.0064 ± 0.0016	1.0 ± 0.14
V108	0.073 ± 0.011	0.067 ± 0.0026	0.93 ± 0.12
A109	0.44 ± 0.035	0.016 ± 0.0036	nd[c]
C110	1.1 ± 0.14	0.11 ± 0.0039	3.9 ± 0.75
E111	0.30 ± 0.020	0.043 ± 0.0092	4.8 ± 0.76
Y115	nd[c]	8.57 ± 1.8	nd[c]
V116	0.15 ± 0.018	nd[c]	0.37 ± 0.041
V118	0.16 ± 0.021	nd[c]	0.49 ± 0.049
H119	2.20 ± 0.27	0.13 ± 0.017	nd[c]
D121	7.3 ± 1.2	0.83 ± 0.082	16 ± 1.2
A122	17 ± 1.8	1.4 ± 0.063	16 ± 1.8
V124	4.8 ± 0.48	0.43 ± 0.019	3.2 ± 0.27

[a] Only residues for which a value of k_{ex} could be determined for either wild-type RNase A or [C40A, C95A] RNase A at pD 5.0 are listed. [b] All errors are reported at the 95% confidence level. [c] Not determined. The corresponding amide $^2H/^1H$ exchange rate was either too large, or the quality of the data was insufficient to measure k_{ex}.

site was slow enough to be observed in [C40A, C95A] RNase A at 12 °C and pD 5.0, but not slow enough to be observed in the more stable wild-type protein at 35 °C and pD 5.0. However, since the value of k_{ex} (8.6×10^{-5} sec^{-1}) for Y115 in [C40A, C95A] RNase A at 12 °C and pD 5.0 was one of the largest values of k_{ex} measured for the mutant protein, and since values of k_{ex} larger than 1×10^{-4} sec^{-1} are difficult to observe by amide $^2H/^1H$ exchange measurements, the difference in k_{ex} for Y115 between [C40A, C95A] RNase A and wild-type RNase A could be quite small. Since the $^2H/^1H$ exchange rate for Y115 in wild-type RNase A at 35 °C could not be measured, a comparison of local stability between mutant and wild-type RNase A in the region of this residue cannot be made.

A summary of individual residue opening free energies (ΔG°_{op}), corrected for proline cis/trans isomerization for the reasons described above, is shown in Figure 3 for [C40A, C95A] RNase A and wild-type RNase A**.** For the purpose of this discussion, we define a quantity $\Omega \equiv \Delta G^\circ_{op}/\Delta G^\circ_{unf}$ (H_2O), with Ω being a direct measure of the relative stability of a given amide site compared to the global stability [characterized by the unfolding free energy, $\Delta G^\circ_{unf}(H_2O)$ under the same conditions of pH and temperature of the respective RNase A form]. A value $\Omega \approx 1.0$ indicates that the unfolding event detected by $^2H/^1H$ exchange is identical to the global unfolding process; i.e., $\Omega \approx \Omega_{global}$. Considering the uncertainties of these experimental measurements, we define values of $\Omega > 0.85$ as evidence that the mechanism of local amide proton exchange involves the global unfolding process. This regime is indicated by the horizontal dashed lines in Figure 3. It should be emphasized that the lower limit of Ω that distinguishes global from subglobal or localized disruptions cannot be defined precisely because of uncertainties in both the GdnHCl unfolding and $^2H/^1H$ exchange data, but that this delineation of the global unfolding regime is reasonable given the precision of the available data. Amide protons of the interstrand hydrogen bonds of β-sheets with values of $\Omega > 0.85$, together with more rapidly exchanging amide sites, are also indicated in the schematic diagrams of Figure 4. Comparison of the data of Figures 3 and 4 for wild-type RNaseA (35 °C), [C40A, C95A] RNase A (12 °C), and [C40A, C95A] RNase A (20 °C) provides information about the distributions of amide sites that exchange by means of a global unfolding process in these protein structures.

Examination of the data presented in Figure 3 reveals that, for both protein forms, some amide sites have values of ΔG°_{op} equal to, or approaching, the corresponding value of $\Delta G^\circ_{unf}(H_2O)$ determined from GdnHCl denaturation experiments ($\Omega = 0.86-1.02$). These sites are characterized as being within the global unfolding regime of the respective RNase A protein form ($\Omega \approx \Omega_{global}$). The largest number of such sites (a total of 23) was found in the wild-type protein at 35 °C, while 15 were observed in [C40A, C95A] RNase A at 12 °C, and only 2 in the same protein at 20 °C. Sites with $\Omega \approx \Omega_{global}$ are located mainly in regions of hydrogen-bonded regular backbone structure in the proteins (e.g., within α-helices or β-sheets; see Figures 3 and 4). It is clear from the data summarized in Figures 3 and 4 that both the wild-type protein at 35 °C and [C40A, C95A] RNase A at 12 °C have numerous amide sites that become accessible to solvent $^2H/^1H$ exchange only when the polypeptide chain experiences a global (or near global) unfolding event. By contrast, with the exception of S59 and C72, [C40A, C95A] RNase A at 20 °C is characterized primarily by amide sites with Ω values indicating subglobal or local conformational fluctuations ($\Omega < 0.85$).

Summaries of Ω values for amide protons within the two β-sheets of [C40A, C95A] RNase A at 20 and 12 °C and wild-type RNase A at 35 °C are presented in Figure 4. The polypeptide segment C72−S75 within strand $\beta 3$[2] of β-sheet 2 (*38*) is one of the most stable structures in [C40A, C95A] RNase A, with the C72, Q74, and S75 sites having values of Ω at or near Ω_{global} at 12 °C (Figure 4B). At 20 °C, the stability of the Q74 residue of [C40A, C95A] RNase A is greatly reduced, leaving only the C72 and S75 amide sites in this mutant with Ω values at or near Ω_{global} (Figure 4A). Comparing data for [C40A, C95A] RNase A shown in Figures 3 and 4, the five residues (I106, A109, C110, E111, and H119) in strands $\beta 6$ and $\beta 7$ near the β-hairpin turn in β-sheet 2 are in the global regime at 12 °C, while none of these amide sites has a value of $\Omega \approx \Omega_{global}$ in this mutant at 20 °C (the A109 and H119 resonances were not observed in the HSQC spectra at 20 °C). Similarly, in the third α-helix (α3), amide sites within polypeptide segment V54−S59 have values of $\Omega \approx \Omega_{global}$ in [C40A, C95A] RNase A at 12 °C, while at 20 °C these same amide sites (except for the S59 site in α3 that is adjacent to β-strand $\beta 3$ in the three-dimensional structure) exchange more rapidly than predicted by global unfolding. Finally, an Ω_{global} value that is observed for M30 in [C40A, C95A] RNase A at 12 °C is reduced significantly in the same mutant at 20 °C ($\Delta\Omega_{[C40A,C95A](12\ °C)-(20\ °C)} = 0.15$ for M30; see Figures 3 and 4 A and B). From the data presented here, it appears that the region that encompasses the small β-strand $\beta 3$ and the C-terminal portion of helix α3 forms the core of most stable residues in [C40A, C95A] RNase A at 20 °C. Under strongly native conditions at 12 °C ($T_m - T = 20$ °C), this core expands to include residues in strands $\beta 6$ (I106, A109, C110, and E111) and $\beta 7$ (H119) of sheet-2, along with a longer stretch of helix α3 (V54−S59).

In wild-type RNase A at 35 °C, all of the amide sites of strand $\beta 3$ (i.e., N71−S75), with the exception of N71, are in the global-unfolding exchange regime ($\Omega \approx \Omega_{global}$, Figure 4). Numerous sites in the C-terminal region of helix α3 (including Q55, C58, S59, and Q60) also have values of $\Omega > 0.85$. In particular, most amide sites identified in the global-unfolding exchange regime for [C40A, C95A] RNase A also exhibit values of $\Omega > 0.85$ in wild-type RNase A (Figures 3 and 4). Interestingly, amide sites of residues A109, C110, and H119 shift from the global-unfolding exchange regime ($\Omega > 0.85$) in [C40A, C95A] RNase A at 12 °C into the subglobal unfolding regime ($\Omega \leq 0.85$) in wild-type RNase A at 35 °C. These changes, in the vicinity of a β-hairpin structure of β-sheet 2, suggest that this hairpin structure has less local conformational fluctuations in the structure of the des-[40−95] intermediate at 12 °C than in the wild-type protein at 35 °C. Amide sites of residues V54

[2] The designations of helices and β-sheets used in this study are based on the locations of α-helices and β-strands reported in the Brookhaven Protein Data Bank (PDB) entry 7RSA: $\beta 1$, sheet 1 strand 1; $\beta 2$, sheet 2 strand 1; $\beta 3$, sheet 2 strand 2; $\beta 4$, sheet 1 strand 2; $\beta 5$, sheet 1 strand 3; $\beta 6$, sheet 2 strand 3; $\beta 7$, sheet 2 strand 4; α1, helix 1; α2, helix 2; α3 helix3.

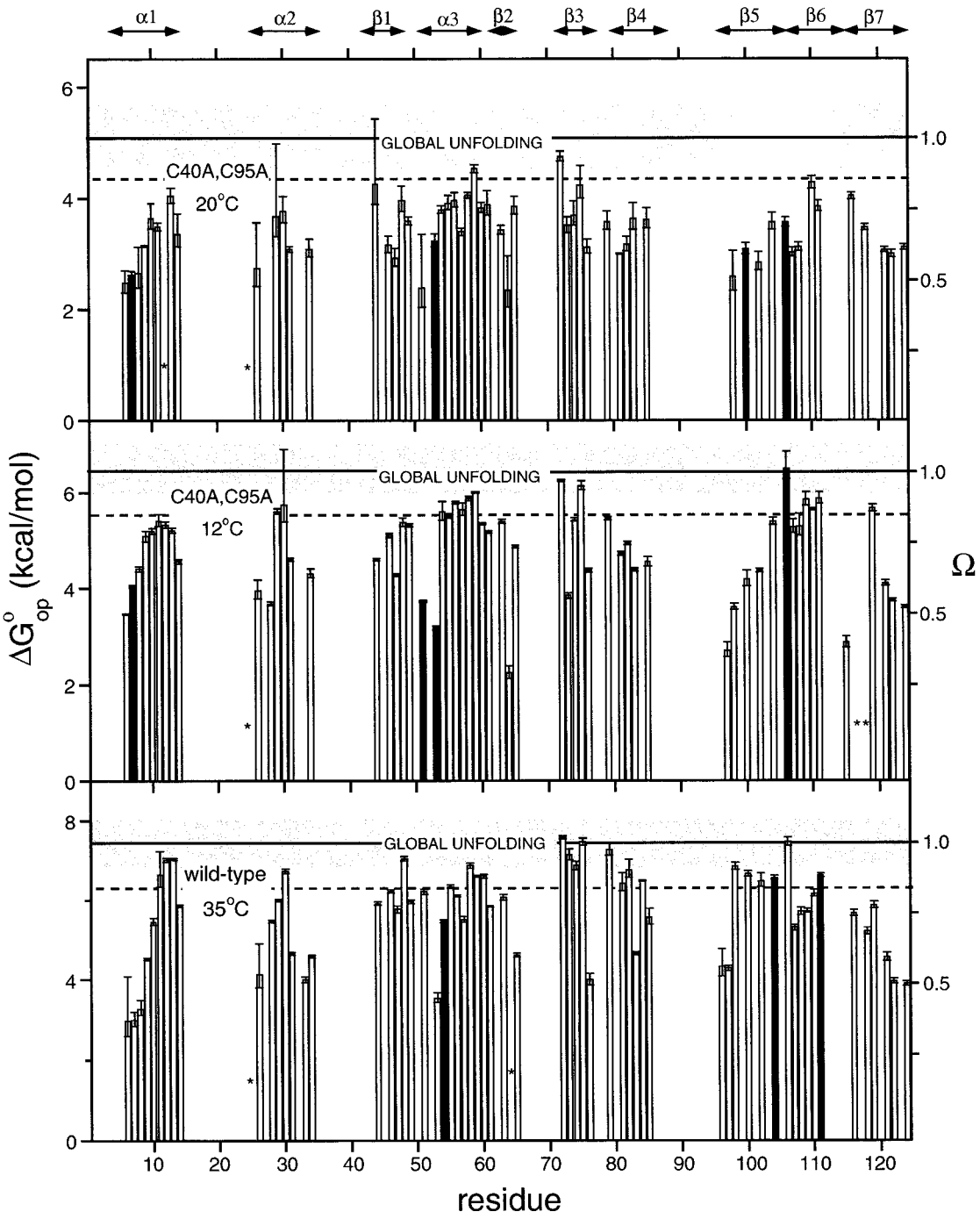

FIGURE 3: Bar plots for [C40A, C95A] RNase A at 20 °C (top), 12 °C (middle), and wild-type RNase A at 35 °C (bottom) of ΔG°_{op} (left axis) and $\Omega \equiv \Delta G^\circ_{op}/\Delta G^\circ_{unf}(H_2O)$ (right axis) for all slowly exchanging backbone amide sites. Error symbols represent the respective uncertainties (at the 95% confidence level) in the linear fits for k_{ex} using eq 5. Values of ΔG°_{op} for individual residues, for which the corresponding NMR $^1H-^{15}N$ resonance assignment was ambiguous, are indicated by solid bars. The value of the global unfolding free energy [$\Delta G^\circ_{unf}(H_2O)$] of each protein form, including the 1.7 kcal/mol correction for proline isomerization, is indicated by a horizontal line on the respective plot, which is bracketed by a shaded region that represents the respective uncertainties (at the 95% confidence level) of these measurements (see Table 1). Horizontal dashed lines correspond to values of $\Omega = 0.85$; amide sites with values of ΔG°_{op} above this dashed line are considered to be in the global-unfolding exchange regime. α-helical and β-sheet regions, from X-ray (*38*) and NMR (*10*, *11*) data for wild-type and mutant RNase A, respectively, are indicated with double-headed arrows above the plot.

and V57 in helix α3 also have values $\Omega \approx \Omega_{global}$ in [C40A, C95A] RNase A at 12 °C, but $\Omega < 0.85$ in wild-type RNase A, indicating less local conformational fluctuations at these sites in this analogue of a folding intermediate than in the folded wild-type protein.

In wild-type RNase A at 35 °C (Figure 4C), β-sheet 1, which consists of strands β1, β4, and β5, has nine residues in the global unfolding regime ($\Omega \approx \Omega_{global}$). By contrast, none of the corresponding residues of the des-[40−95] analogue at 12 °C (Figure 4B) or 20 °C (Figure 4A) has values of $\Omega \approx \Omega_{global}$. Sites which exhibit significant differences in global vs local exchange mechanisms between wild-type and [C40A, C95A] RNase A include amide protons of residue H48 in strand β1, residues M79, I81, T82, and C84 of strand β4, residues K98, T100, A102, and K104 of strand β5, and also residues Q11, H12, and M13 within helix

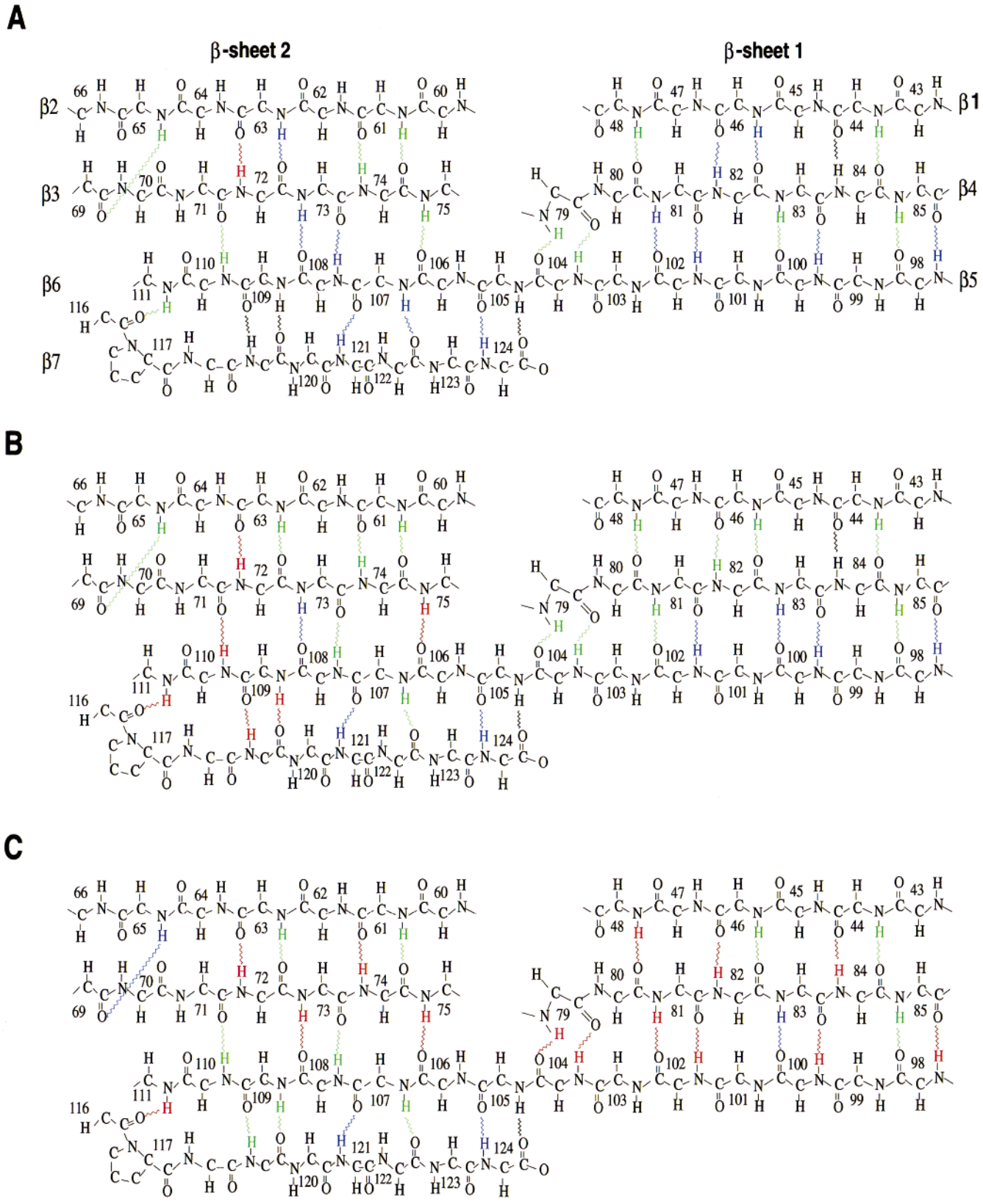

FIGURE 4: Relative stability $\Omega \equiv \Delta G^{\circ}_{op}/\Delta G^{\circ}_{unf}(H_2O)$ of individual residues for [C40A, C95A] RNase A at (A) 20 °C and (B) 12 °C, and for (C) wild-type RNase A at 35 °C, superimposed on a schematic representation of the two β-sheet structures (i.e., β-sheet 1 consists of β1, β4, and β5 and β-sheet 2 includes β2, β3, β6, and β7; see A) of wild-type RNase A (*38*). Values of ΔG°_{op} for mutant and wild-type RNase A were measured at pD 5.0, while corresponding values of $\Delta G^{\circ}_{unf}(H_2O)$ were determined at pH 4.6. Wavy lines represent hydrogen bonds with donors from residues with the relative stability indicated by using different colors as follows: $\Omega > 0.85$ (red), $0.85 \geq \Omega > 0.70$ (green), and $0.70 \geq \Omega$ (blue). Hydrogen bonds in the X-ray structure of the wild-type protein, which were not observed experimentally by $^2H/^1H$ exchange, are indicated by black wavy lines.

α1. Compared to the disulfide-intact wild-type protein at 35 °C, significant differences exist in local structural fluctuations and stability within β-sheet 1 and helix α1 of the des-[40−95] analogue at 12 and 20 °C.

DISCUSSION

The global [$\Delta G^\circ_{unf}(H_2O)$] and local ($\Delta G^\circ_{op}$) stability of both wild-type RNase A and an analogue of the disulfide-folding intermediate lacking the C40−C95 bond have been characterized. There were several purposes for measuring these unfolding free energies at pH 4.6 over the selected temperature ranges (20, 25, 30, and 35 °C for wild-type, and 12, 16, 20, and 24 °C for [C40A, C95A] RNase A). First, by measuring $\Delta G^\circ_{unf}(H_2O)$ at 20 °C for both mutant and wild-type RNase A, a direct comparison of the overall thermodynamic stabilities of the respective protein forms could be assessed (*39*). Second, since three-dimensional structures of both protein forms have been characterized previously (*10*, *11*, *38*), analysis of local conformational fluctuations and stability based on amide $^2H/^1H$ exchange measurements complements the structural data and provides a more complete picture of the structural and dynamic basis of the relative overall stabilities of des-[40−95] RNaseA and wild-type RNase A. Finally, comparison of $\Delta G^\circ_{unf}(H_2O)$ with the individual site-specific unfolding free energies (ΔG°_{op}) for the des-[40−95] analogue, measured under strongly native conditions (12 °C), and more destabilizing conditions (20 °C), provides insights as to which regions of RNase A are stabilized during the course of the major conformational folding step in RNase A (3S ⇔ des-[40−95]; Figure 1). Similarly, comparison of the same parameters for the mutant and wild-type proteins under strongly native conditions for both forms (e.g., 12 °C for [C40A, C95A] RNase A and 35 °C for wild-type RNase A) can be used to determine which regions of the proteins are stabilized in the folding step from des-[40−95] to native RNase A (Figure 1).

Any residue of des-[40−95] RNase A that has a value of $\Omega \approx \Omega_{global} \approx 1$ (defined here by assigning a range of values of 0.86−1.02 to Ω_{global} for this study; see Results) at a temperature that strongly favors the native structure (12 °C), and a lower value of Ω at a higher temperature (20 °C), is postulated to have undergone a change from global to subglobal or local amide $^2H/^1H$ exchange somewhere in this temperature range. This trend toward a reduced value of Ω with increased destabilization of the protein suggests that intramolecular interactions at or near amide sites with this behavior are important in stabilizing the des-[40−95] RNase A folding intermediate relative to 3S. Moreover, Bai and Englander (*40*) have shown that cooperative structural folding units exist in cytochrome *c* that contain residues with similar trends in Ω values as a function of increased denaturant concentration (e.g., increased destabilization of the native structure). While such cooperative structural folding units have not been identified in RNase A, residues of the des-[40−95] RNase A analogue with similar trends in Ω as a function of temperature would suggest the possibility of cooperativity of these residues in the 3S ⇔ des-[40−95] folding step. However, a detailed investigation of Ω as a function of temperature (or denaturant concentration) would be necessary to determine whether these residues acted cooperatively or independently in the folding process. Such an analysis is beyond the scope of this work because of the limitation that $^2H/^1H$ exchange rates could not be measured accurately over a wide temperature range.

Following the reasoning in the preceding paragraph, an amide site that is *not* initially in the global regime of $^2H/^1H$ exchange in des-[40−95] RNase A ($\Omega < \Omega_{global}$), but acquires a value of $\Omega \approx \Omega_{global}$ after some stabilizing event such as the formation of the Cys40−Cys95 disulfide cross-link to form native wild-type RNase, must have changed to a mode of amide proton exchange characterized by global unfolding. Therefore, residues with amide sites exhibiting this trend in Ω as a function of disulfide-bond formation, are postulated to be crucial in stabilizing the global native structure. Moreover, the specific interresidue interactions that facilitate the final des-[40−95] ⇒ N folding step are likely to be contained in those specific regions of the protein in which Ω increased to Ω_{global} upon formation of the Cys40−Cys95 disulfide bond. It should be emphasized that the objective here is to identify specific residues that are important in the des-[40−95] ⇒ N folding step in the oxidative folding of RNase A under strongly native conditions (e.g., at the temperature and pH regimes at which the native protein is energetically favored). To achieve this favorable protein stability, the temperatures chosen to study [C40A, C95A] RNase A (12 °C) and wild-type RNase A (35 °C) were approximately the same distance ($T_m - T \sim$ 20 °C) from their respective T_m's ($T_{m[wild\text{-}type]} = 55.5$ °C and $T_{m\ [C40A,\ C95A]} = 33.5$ °C) (*10*, *11*). Under these conditions, the changes in stability of the individual amide sites, upon formation of the Cys40−Cys95 disulfide bond, are likely to reflect specific localized stabilizing effects of this covalent disulfide cross-link in the folding of RNase A through the major oxidative regeneration pathway.

Sources of Uncertainties. Inaccuracies in the measured values of $\Delta G^\circ_{unf}(H_2O)$ could, in principle, be problematic in this analysis. If the value of $\Delta G^\circ_{unf}(H_2O)$ were underestimated, then numerous sites would likely have values of ΔG°_{op} significantly greater than $\Delta G^\circ_{unf}(H_2O)$, which was not the case. On the other hand, if $\Delta G^\circ_{unf}(H_2O)$ were overestimated for both wild-type RNase A at 35 °C and [C40A, C95A] RNase A at 12 and 20 °C, then the major implication of this erroneous measurement would be that the $^2H/^1H$ exchange at most or all amide sites of RNase A is governed by subglobal, rather than global fluctuations. The specific amide sites identified as being in the global unfolding regime ($\Omega \approx \Omega_{global}$) would still be the most stable amide sites in the protein. However, if $\Delta G^\circ_{unf}(H_2O)$ were overestimated for the wild-type protein at 35 °C, but not overestimated for the mutant protein at 12 and/or 20 °C, or vice versa, then the relative number of sites in each protein for which $\Omega \approx \Omega_{global}$ would be different. This type of error would result in an incorrect interpretation of the relative values of Ω for the mutant and wild-type RNase A. However, given that the most stable sites in both wild-type RNase A at 35 °C and [C40A, C95A] RNase A at 12 and 20 °C have Ω values near 1 (Figure 4), it seems unlikely that $\Delta G^\circ_{unf}(H_2O)$ for mutant RNase A (at 12 and 20 °C) or wild-type RNase A (at 35 °C) was overestimated significantly.

Finally, regarding deuterium isotope effects on comparing the measured local stability (ΔG°_{op}) of RNase A in D_2O with the corresponding global $\Delta G^\circ_{unf}(H_2O)$ value in H_2O, these effects have been measured (Laity, J. H., Hao, M., Juminaga, D., and Scheraga, H. A., in preparation) and determined to be small [much less than the respective uncertainties in $\Delta G^\circ_{unf}(H_2O)$]. Furthermore, it was deter-

mined that the global stability for both mutant and wild-type RNase A is most similar in ^1H_2O and ^2H_2O when compared at pH 4.6 and pD 5.0, respectively. This result is consistent with measurements of deuterium isotope effects on the shift of amino acid side-chain pK_a's by Bundi and Wüthrich (*41*), in which it was determined that the stability of a protein in D_2O and H_2O is most similar when $pH_{H_2O} = pH_{read(D_2O)}$ (where $pH_{read(D_2O)} = pD - 0.4$, eq 1). Therefore, GdnHCl data [to obtain $\Delta G^\circ_{unf}(H_2O)$] were determined at pH 4.6, and $^2H/^1H$ exchange data (to obtain ΔG°_{op}) were recorded at pD 5.0 for both wild-type and [C40A, C95A] RNase A.

Global Thermodynamic Parameters. The relative stability of the global chain fold of [C40A, C95A] RNase A has been compared quantitatively to the wild-type protein at pH 4.6 and 20 °C. Using the method of overlapping loops (*42*), a quantitative estimation of the difference in loop entropies $[\Delta\Delta\mu^\circ_{conf(loop)}]$ of the denatured states of wild-type and mutant RNase A can be made. Comparison of $\Delta\Delta\mu^\circ_{conf(loop)}$ to the difference in the global unfolding free energies of the two proteins $[\Delta\Delta G^\circ_{unf}(H_2O)]_{wild\text{-}type-[C40A,C95A]} = \Delta\Delta\mu^\circ_{conf(experimental)}]$ can elucidate the relative contribution of disulfide-bond formation in entropically destabilizing the unfolded state (*42*). The value for $\Delta\Delta\mu^\circ_{conf(experimental)}$ is 4.55 ± 0.95 kcal/mol (at the 95% confidence level, Table 1) at 20 °C, compared to a $\Delta\Delta\mu^\circ_{conf(loop)}$ of 4.0 kcal/mol calculated at the same temperature. This small difference of 0.55 kcal/mol at 20 °C is not significant within the experimental error (±0.95 kcal/mol for $\Delta\Delta\mu^\circ_{conf(experimental)}$), and within the theoretical error arising from the approximation of applying Gaussian distributions to short chains in the loop entropy calculation to determine $\Delta\Delta\mu^\circ_{conf}$(42). Accordingly, these data support the view that the primary effect of forming the C40−C95 disulfide cross-link in the final step of the major regeneration pathway of RNase A is the inherent destabilization of the unfolded state of the protein relative to the native state, arising from the decreased entropy of the denatured state.

The 3S ⇔ des-[40−95] Folding Step. The individual unfolding free energies (ΔG°_{op}) were calculated with high precision (see error symbols in Figure 3) for many residues with slowly exchanging amide sites in wild-type and [C40A, C95A] RNase A. From a comparison of these measurements at different temperatures for [C40A, C95A] RNase A, and a comparison of the same measurements for the mutant and wild-type forms, we can infer the location of the most stable regions of the two protein forms. From this information, the implications for the major folding pathway from 3S through des-[40−95], in terms of stabilizing the intermediate and native forms, can be inferred. Given that the Ω values measured for Cys72 show that this amide site is in the global regime ($\Omega \approx \Omega_{global}$) in the des-[40−95] analogue, even under conditions (20 °C and pD 5.0) in which most other sites in the protein are not, it appears that some locally stabilizing interactions, possibly in addition to the hydrogen bonding shown in Figure 4, occur in this region in the 3S ⇔ des-[40−95] folding step. Moreover, Figure 4 shows that the amide site of residue Cys65 reaches its maximum relative stability in des-[40−95] RNase A ($\Omega_{C65\ [C40A,\ C95A]\ RNase\ A\ 20\ and\ 12\ °C} > \Omega_{C65\ wild\text{-}type\ RNase\ A\ 35\ °C}$). Collectively, these results are consistent with earlier observations that this region of RNase A has local structure that is stabilized by local interactions early in the conformational folding process (e.g., from the earliest conformational events that characterize the 3S ⇔ des-[40−95] folding step) (*5*, *9*, *43*).

Another region of RNase A that may stabilize des-[40−95] during this same folding step is β-sheet 2 near the β-hairpin turn at P117, consisting of β6 and β7 (Figures 3 and 4). Five residues in this region (I106, A109, C110, E111, and H119) are in the global regime ($\Omega \approx \Omega_{global}$) in the des-[40−95] analogue at 12 °C. In addition, three of these residues, A109, C110, and H119, reach maximum relative stability compared to the wild-type protein in [C40A, C95A] RNase A at 12 °C (the same residues are not in the global regime in the wild-type protein). All five of the residues in β6 and β7 are much less stable at 20 °C in the mutant form (A109 and H119 are not even observed in the HSQC spectrum at 20 °C). The region of RNase A consisting of helix α3, shown in Figure 3, exhibits a very similar trend in Ω. All together, these data suggest that these two regions of the protein are (i) important in stabilizing the des-[40−95] fold, which forms in the rate-determining step on the major oxidative folding pathway, and (ii) may encompass residues that provide intramolecular interactions in these regions which drive these folding events. Significantly, the α3 region of RNase A also appears to play a role in stabilizing the native fold of the protein, since most of the residues in helix α3 of the wild-type protein are still in the global regime (Figure 3). Another local region of the protein, which reaches global stability in the des-[40−95] analogue at 12 °C and remains in this regime in the native protein, is M30 in helix α2. This residue stabilizes the des-[40−95] analogue and may ultimately influence the folding step, through unknown intramolecular contacts.

Stabilization of the Native Fold. It is evident from Figure 4C that the region of β-sheet 1 in native wild-type RNase A is one of the most stable regions in the protein, with nine hydrogen bonding residues (M79, I81, T82, C84, K98, T100, A102, K104, and H48) in the global stability class. More striking is the profound destabilization of this same region in the des-[40−95] analogue, even under strongly native conditions (12 °C, Figure 4B). These data demonstrate that the redox-dependent, fast-folding step, involving formation of the Cys40−Cys95 disulfide cross-link in des-[40−95], results in the formation of, or significant increase in the number of residues involving a core region of global stability in the native wild-type protein. In addition, intramolecular interactions *within* and *between* the first α-helix and the first β-sheet of the protein may also be important factors in stabilizing the native fold in the final step through the des-[40−95] pathway; i.e., the correlated conversion of Ω from subglobal or local relative stability to Ω_{global} for the residues in β-sheet 1 (M79, I81, T82, C84, K98, T100, A102, K104, and H48) and helix α1 (Q11, H12, and M13) during the des-[40−95] ⇒ N folding step (Figures 3 and 4) suggests that the specific regions encompassing these residues may contain key intramolecular contacts which drive this final folding step. Moreover, the close proximity of helix α1 to β-sheet 1 in the native three-dimensional structure (*38*) suggests that the correlated stabilization of residues in these two secondary structures in the des-[40−95] ⇒ N folding step is important for stabilizing the folded native structure of wild-type RNase A.

CONCLUSIONS

In this study, we have compared amide $^2H/^1H$ exchange and global stability in an analogue of an oxidative folding intermediate with that of the wild-type protein. Results of this comparison suggest that conformational folding of RNase A is stabilized by local interactions and conformational dynamics in distinct regions of the polypeptide chain. As protein folding progresses along the major pathway involving the des-[40−95] folding intermediate, the locations of these regions change. In particular, specific regions that we propose are crucial for stabilizing the native structure of wild-type RNase A and of the des-[40−95] folding intermediate have been identified, and the distributions of hydrogen-bonded amide sites in these proteins exhibiting local conformational fluctuations (i.e., proton exchange via subglobal unfolding events) have been characterized. These conformational dynamics contribute to the relative stabilities of 3S, des-[40−95], and N species along the major oxidative folding pathway. We also observed that most of the stabilization of the native structure that occurs in the final folding step (des-[40−95] ⟹ N) can be attributed to the decrease in conformational entropy of the unfolded state due to formation of the Cys40−Cys95 disulfide bond. Collectively, these observations provide new insights regarding specific regions and interactions within RNase A that are crucial in determining the relative stabilities of species along the major pathway for oxidative folding.

ACKNOWLEDGMENT

We thank M. A. McDonald for assistance in cloning the plasmids to express recombinant [C40A, C95A] RNase A, V. G. Davenport, C. C. Lester, and T. W. Thannhauser for technical assistance, and S. Shimotakahara for many helpful discussions.

SUPPORTING INFORMATION AVAILABLE

Table S1 and S2, temperature dependence of ^1H- and ^{15}N-resonance assignments for wild-type and [C40A, C95A] RNase A, respectively.

REFERENCES

1. Hantgen, R. R., Hammes, G. G., and Scheraga, H. A. (1974) *Biochemistry 13*, 3421−3431.
2. Ahmed, A. K., Schaffer, S. W., and Wetlaufer, D. B. (1975) *J. Biol. Chem. 250*, 8477−8482.
3. Creighton, T. E. (1977) *J. Mol. Biol. 113*, 329−341.
4. Konishi, Y., Ooi, T., and Scheraga, H. A. (1981) *Biochemistry 20*, 3945−3955. (b) Konishi, Y., Ooi, T., and Scheraga, H. A. (1982) *Biochemistry 21*, 4734−4740. (c) Konishi, Y., Ooi, T., and Scheraga, H. A. (1982) *Biochemistry 21*, 4741−4748. (d) Konishi, Y., Ooi, T., and Scheraga, H. A. (1982) *Proc. Natl. Acad. Sci. U.S.A 79*, 5734−5738.
5. Altmann, K.-H., and Scheraga, H. A. (1990) *J. Am. Chem. Soc. 112*, 4926−4931.
6. Lester, C. C., Xu, X., Laity, J. H., Shimotakahata, S., and Scheraga, H. A. (1997) *Biochemistry 36*, 13068−13076.
7. (a) Rothwarf, D. M. and Scheraga, H. A. (1991) *J. Am. Chem. Soc.* 113, 6293−6294. (b) Rothwarf, D. M., and Scheraga, H. A. (1993) *Biochemistry 32*, 2671−2679. (c) Rothwarf, D. M., and Scheraga, H. A. (1993) *Biochemistry 32*, 2680−2689. (d) Rothwarf, D. M., and Scheraga, H. A. (1993) *Biochemistry 32*, 2690−2697. (e) Rothwarf, D. M., and Scheraga, H. A. (1993) *Biochemistry 32*, 2698−2703. (f) Rothwarf, D. M., Li, Y.-J., and Scheraga, H. A. (1998) *Biochemistry 37*, 3760−3766. (g) Rothwarf, D. M., Li, Y.-J., and Scheraga, H. A. (1998) *Biochemistry 37*, 3767−3776.
8. Iwaoka, M., Juminaga, D., and Scheraga, H. A. (1998) *Biochemistry 37*, 4490−4501.
9. Xu, X., and Scheraga, H. A. (1998) *Biochemistry 37*, 7561−7571.
10. Shimotakahara, S., Rios, C. B., Laity, J. H., Zimmerman, D. E., Scheraga, H. A., and Montelione, G. T. (1997) *Biochemistry* 36, 6915−6929.
11. Laity, J. H., Lester, C. C., Shimotakahara, S., Zimmerman, D. E., Montelione, G. T., and Scheraga, H. A. (1997) *Biochemistry* 36, 12683−12699.
12. Nozaki, Y. (1972) *Methods Enzymol. 26*, 43−50.
13. Laity, J. H., Shimotakahara, S., and Scheraga, H. A. (1993) *Proc. Natl. Acad. Sci. U.S.A 90*, 615−619.
14. delCardayré, S. B., Ribó, M., Yokel, E. M., Quirk, D. J., Rutter, W. J., and Raines, R. T. (1995) *Protein Eng. 8*, 261−273.
15. Glasoe, P. K., and Long, F. A. (1960) *J. Phys. Chem. 64*, 188−190.
16. Denton, J. B., Konishi, Y., and Scheraga, H. A. (1982) *Biochemistry 21*, 5155−5163.
17. Santoro, M. M., and Bolen, D. W. (1988) *Biochemistry 27*, 8063−8086.
18. Nagayama, K., (1986) *J. Magn. Reson. 69*, 508−510.
19. Kay, L. E., Keifer, P., and Saarinen, T. (1992) *J. Am. Chem. Soc. 114*, 10663−10665.
20. Wishart, D. S., Bigam, C. G., Yao, J., Abildgaard, F., Dyson, H. J., Oldfield, E., Markley, J. L., and Sykes, B. D. (1995) *J. Biomol. NMR 6*, 135−140.
21. Grzesiek, S., and Bax, A. (1993) *J. Biomol. NMR 3*, 627−638.
22. Hvidt, A., and Nielsen, S. O. (1966) *Adv. Protein Chem. 21*, 287−386.
23. Hilton, B. D., and Woodward, C. K. (1979) *Biochemistry 18*, 5834−5841.
24. Englander, S. W., and Kallenbach, N. R. (1984) *Quart. Rev. Biophys. 16*, 521−655.
25. Roder, H., Wagner, G., and Wüthrich, K. (1985) *Biochemistry 24*, 7396−7407.
26. Molday, R. S., Englander, S. W., and Kallen, R. G. (1972) *Biochemistry 11*, 150−158.
27. Bai, Y., Milne, J. S., Mayne, L., and Englander, S. W. (1993) *Proteins 17*, 75−86.
28. Englander, J. J., Calhoun, D. B., and Englander, S. W. (1979) *Anal. Biochem. 92*, 517−524.
29. Gregory, R. B., Crabo, L., Percy, A. J., and Rosenberg, A. (1983) *Biochemistry 22*, 910−917.
30. Nall, B. T. (1985) *Comments Mol. Cell. Biophys. 3*, 123−143.
31. Tanford, C. (1970) *Adv. Protein Chem. 24*, 1−95.
32. Brandts, J. F., Halvorson, H. R., and Brennan, M. (1975) *Biochemistry 14*, 4953−4963.
33. Adler, M., and Scheraga, H. A. (1990) *Biochemistry 29*, 8211−8216.
34. (a) Houry, W. A., Rothwarf, D. M., and Scheraga, H. A. (1994) *Biochmistry 33*, 2516−2530. (b) Houry, W. A., Rothwarf, D. M., and Scheraga (1995) *Nature Struct. Biol. 2*, 495−503.
35. Bai, Y., Milne, J. S., Mayne, L., and Englander, S. W. (1994) *Proteins 20*, 4−14.
36. Juminaga, D., Wedemeyer, W. J., and Scheraga, H. A. (1998) *Biochemistry 37*, 11614−11620.
37. Hermans, J., and Scheraga, H. A. (1961) *J. Am. Chem. Soc. 83*, 3283−3292.
38. Wlodawer, A., Svensson, L. A., Sjölin, L., and Gilliland, G. L. (1988) *Biochemistry 27*, 2705−2717.
39. Iwaoka, M., Wedemeyer, W. J., and Scheraga, H. A. (1999) *Biochemistry* 38, 2805−2815.
40. Bai, Y., and Englander, S. W. (1996) *Proteins 24*, 145−151.
41. Bundi, A., and Wüthrich, K. (1977) *FEBS Lett.. 77*, 11−14.
42. Lin, S. H., Konishi, Y., Denton, M. E., and Scheraga, H. A. (1984) *Biochemistry 23*, 5504−5512.
43. Montelione, G. T., and Scheraga, H. A. (1989) *Acc. Chem. Res. 22*, 70−76.

BI9911684